The effect of channel tributaries on the evolution of submarine channel confluences (Espírito Santo Basin, SE Brazil)

Yongpeng Qin [1 2 3], Tiago M. Alves [3], José Antonio Constantine [4], Davide Gamboa [5], Shiguo Wu [1 2]

[1] Laboratory of Marine Geophysics and Geo-resources, Institute of Deep-sea Science and Engineering, Chinese Academy of Sciences, Sanya, 572000, China. Email: qinyp@idsse.ac.cn.

[2] Laboratory for Marine Geology, Qingdao National Laboratory for Marine Science and Technology, Qingdao, 266061, China.

[3] 3D Seismic Lab, School of Earth and Ocean Sciences, Cardiff University, Main Building, Park Place, Cardiff, CF10 3AT, United Kingdom.

[4] Department of Geosciences, Williams College, Clark Hall, 947 Main Street, Williamstown, MA01267, United States of America.

[5] British Geological Survey, Room 0.73, Cardiff University, Main Building, Park Place, Cardiff, CF10 3AT, United Kingdom.

ABSTRACT

Confluences are geomorphologic features fed by distinct channel tributaries and record the contribution of multiple sediment sources. They are key features of both fluvial and submarine channels in geomorphologic and sedimentologic terms. Here, we use high-quality 3D seismic data from SE Brazil to document the response of a submarine channel confluence to turbidity currents sourced from a tributary. The studied channel system consists of a west tributary, an east tributary and a post-confluence channel, with the last two comprising the main channel at present. Downstream from the confluence, a series of changes in planform morphology and architecture were found due to the effect of turbidity currents sourced from the west tributary channel. A channel bend in the main channel curved toward the west when it was first formed but later curved toward the east, and so remained until the present day. This process led to the migration of the confluence point ~500 m to the east, and changed its bed morphology from discordant (the beds of tributaries and main channels meet at an unequal depth) to concordant (the beds of tributaries and main channels meet at approximately the same depth). In addition to the channel bend near the confluence, two other bends further downstream record significant changes with time, increasing channel sinuosity from 1.11 to 1.72. These three channel bends near the confluence accumulated a large volume of sediment at their inner banks, generating depositional bars. Multiple channel forms within the depositional bars indicate the occurrence of large-scale lateral migration near the confluence. Hence, turbidity currents from the west tributary are shown to influence submarine channels by promoting lateral channel migration, confluence migration, increases in channel sinuosity, and the formation of large depositional bars. The above variations near the confluence reveal a change in tributary activity and a shift in sediment sources from east to west on the continental shelf. Such a shift suggests variations in sedimentary processes on the continental shelf but with unclear causes.

Keywords: SE Brazil; Submarine channel; Confluence; Tributary; Lateral migration; Sediment supply

INTRODUCTION

Confluences mark the locations where two channels meet to accommodate water and sediment flows from distinct tributaries (e.g. Best, 1987; Ferguson and Hoy, 2008; Ismail, 2017). In fluvial channels, the varied depositional records upstream and downstream of confluences reflect the contribution and provenance evolution of their tributaries (e.g. Constantine et al., 2014; Munack et al., 2014; Jonell et al., 2017). On the Tibetan plateau and Himalayas, for instance, geochemical and sediment-composition analyses of fluvial channel confluences were used to demonstrate variations in the denudation rates of mountain ranges due to climatic, glacial and tectonic events (Munack et al., 2014; Jonell et al., 2017; Munoz et al., 2019). In submarine settings, channels are conduits that transport sediment from land sources to the deep sea (e.g. Kolla et al., 2007; Jobe et al., 2015). Sedimentary records from submarine-channel tributaries and associated confluences reflect variations in the hydrodynamics of turbidity currents sourced from different parts of continental margins. In tectonically active regions such as the Cascadia Margin, North America, turbidite sequences cored upstream and downstream of channel confluences are key for recognising the main triggers of turbidity currents (Goldfinger, 2011; Atwater et al., 2014). Some submarine confluences indicate variations in sedimentary processes on the continental shelf (Jobe et al., 2015; Hansen et al., 2017). Offshore the Niger Delta, the occurrence of a submarine channel tributary and a new confluence may have caused by an avulsion of rivers on Niger Delta (Jobe et al., 2015).

Submarine channel confluences are well documented on continental margins such as West Africa (e.g. Pirmez et al., 2000; Hansen et al., 2017), in North and South America (e.g. Greene et al., 2002; Mitchell, 2004; Paull et al., 2011; Gamboa et al., 2012), offshore Japan (Noda et al., 2008), and in New Zealand (Micallef et al., 2014). On the Atlantic continental slope off New Jersey, Mitchell (2004) observed that tributary canyons tend to be steeper near their confluences than main slope canyons. Similar patterns have been documented in other parts of the USA (Greene et al., 2002), offshore Japan (Noda et al., 2008), in New Zealand (Micallef et al., 2014) and Nigeria (Hansen et al., 2017). In SE

Brazil, the gradients of tributaries and main channels are nearly the same for the Miocene-Quaternary Rio Doce Canyon System (Gamboa et al., 2012). However, channel width and height increase downstream of an Early Miocene channel confluence in the same area considered in this paper (Fig. 1). In Nigeria, a decrease in channel size is recorded downstream of a channel confluence (Jobe et al., 2015), contrasting with the information in Gamboa et al. (2012). Further data from offshore Nigeria recorded changes in channel pathways, and associated sinuosity, near submarine confluences: a) Jobe et al. (2015) described the straightening of a submarine channel downstream of a confluence and attributed it to 'underfit' flows sourced from a tributary, b) Hansen et al. (2017) documented a marked difference in channel sinuosity between a relatively straight tributary (Upper Avon channel) and a sinuous post-confluence channel (Lower Avon channel). This increase in sinuosity relates to the presence of an inherited, but presently inactive, main channel (Hansen et al., 2017).

Morphologic changes in submarine confluences reflect the complex hydrodynamics of submarine channels. Variation in flow dynamics at confluences is probably one main cause for such complexity. For example, there are three possible scenarios when considering flow dynamics at submarine channel confluences (Gamboa et al., 2012): a) confluences showing an active tributary and an active main channel (e.g. Gamboa et al., 2012), b) confluences between an active tributary and an inactive main channel (e.g. Jobe et al., 2015), and c) confluences dominated by an active main channel and an inactive tributary (e.g. Pirmez et al., 2000). Furthermore, tributary flows are able to reactivate abandoned or inactive submarine channels, in which case pattern b) above can be inferred (Jobe et al., 2015; Hansen et al., 2017). Numerical simulations and experimental studies show that junction angles are critical to flow hydrodynamics in submarine confluences (Ismail, 2017). Increases in junction angle from 30° to 90° lead to an increase in the peak front velocity and front thickness of turbidity currents (Ismail, 2017).

Although the morphology and architecture of submarine channel confluences have been extensively documented (Mitchell et al., 2004; Gamboa et al., 2012; Jobe et al., 2015; Hansen et al., 2017), little attention has been paid to: a) confluence evolution through time, and b) the responses of confluences to turbidity currents sourced from channel tributaries.

This work reconstructs the temporal variations in submarine channel morphology around a Pliocene-Quaternary confluence offshore Espírito Santo Basin, SE Brazil (Fig. 1). The studied channel system is commonly named *Rio Doce Canyon, or Channel System,* in the literature (Qin et al., 2016). It is only partly filled by sediment and comprises two tributaries upstream, and a post-confluence channel downstream (Fig. 1B). The continuity of sedimentary infill patterns between the east tributary and the post-confluence channel, as well as their continuous channel thalwegs, indicate that these two channel segments are the main flow pathway at present (Gamboa et al., 2012). There has been a detailed description of spatial changes in morphologic characters of this channel system (Gamboa et al., 2012, Qin et al., 2016), however, the architecture and the temporal evolution of the channel system and the confluence region were not fully addressed in previous work.

We aim at analyzing how submarine channels adjust their morphology and architectures in response to turbidity currents sourced from tributaries. Hence, this paper provides a case study documenting: 1) temporal variations in submarine channel morphology near confluences, and 2) the depositional architecture of a submarine channel system around its confluence region.

DATA AND METHODS

The interpreted 3D seismic volume covers 1600 km^2 of the northern Espírito Santo Basin, SE Brazil (Fig. 1A; Alves et al., 2009), and has a bin spacing of 12.5 m by 12.5 m, with a 2 ms vertical sampling interval. The vertical resolution of the seismic data is ~10 m at the depth of analysis in this study, based on a dominant frequency of 40 Hz and a P-wave velocity of 1600 m/s for near-seafloor strata. This vertical resolution improves to ~ 5 m on the sea floor. A water-column velocity of 1480 m/s is used for time-depth conversions of seafloor features.

Channel depth was measured at intervals of 125 m at the channel thalweg (i.e. the deepest point of channels) along the west tributary and the main channel. The cross-sectional area of the channel system (CSA_E), and cross-sectional area of deposits within the channel system (CSA_D), were calculated at intervals of 1 km along the main channel (i.e. east tributary and post-confluence channel) and exclude overbank deposits (Fig. 2), which may have similar seismic facies to deposits that are not related to channels, and induce errors in geomorphologic calculations. The parameter CSA_E indicates the size of the channel system generated by erosional processes. In turn, CSA_D concerns the sediment volumes accumulated by depositional processes within the channel system. Sediment volume is calculated as CSA_D multiplied by distance along the channel, and is proportional to CSA_D.

The depositional ratio, defined as CSA_D/CSA_E, is used here to quantify sediment dispersal patterns in the studied channel system. This ratio quantifies the percentage of the area filled by deposits at pre-selected sections across the channel system. As flows may deposit more sediment in locations where erosion has produced more accommodation, CSA_D is normalized by CSA_E in order to eliminate the influence of CSA_E on deposition.

GEOLOGIC SETTING

Tectono-sedimentary evolution of the Espírito Santo Basin

The Espírito Santo Basin is located on the continental margin of SE Brazil, between the Abrolhos Bank and the Campos Basin (Fig. 1A). The development of the Espírito Santo Basin is related to the breakup of the Gondwana supercontinent (Ojeda, 1982; Mohriak, 2008), with three main tectono-stratigraphic megasequences filling the basin: syn-rift, transition and drift (França et al., 2007). The 'syn-rift' megasequence spans the Late Berriasian to Early Aptian and comprises fluvial-lacustrine sediments (Ojeda, 1982). The transitional megasequence spans the Middle Aptian to Late Aptian/Early Albian and is composed of thick evaporites and marine carbonates (Ojeda, 1982). Thick salt was deposited at this time to be later deformed into various salt structures (e.g. salt rollers, salt diapirs and salt canopies) by gravitational gliding and differential loading (Fiduk et al., 2004). Salt structures controlled deposition in great part of the Espírito Santo Basin, deforming carbonates accumulated in the transitional megasequence and marine strata of Late Aptian/Early Albian to Holocene age (Ojeda, 1982).

In the study area, two salt ridges bound a NW-SE salt-withdrawal basin containing large-scale depositional elements such as mass-transport deposits (MTDs), turbidite lobes, submarine canyons and channels (Gamboa and Alves, 2015). The distribution and geometry of these depositional elements are closely related to the location of seven (7) distinct salt diapirs that grew close to the modern sea floor (Alves et al., 2009; Gamboa et al., 2012; Gamboa and Alves, 2015).

Sources of sediment to submarine channels

In the Espírito Santo Basin, one possible terrestrial sediment source for the interpreted submarine channels is the Rio Doce (Fig. 1A). This river has an annual suspended-sediment flux of 11 x 10^6 ton/year (Lima et al., 2005), and an annual average discharge of 900 m^3/s (Oliveira et al., 2012). The present-day distance between the mouth of the Rio Doce and the shelf edge is ~ 70 km (Fig. 1A). Turbid river water has been observed 40 km off the Rio Doce after prolonged rainfall, suggesting that hyperpycnal flow events are able to deliver sediment to the continental slope during river floods (Summerhayes et al., 1976).

On the continental shelf, seismic data shows a series of incised valleys connected to the Rio Doce Channel System (Bischoff and Lipski, 2008). However, it seems that these valleys are no longer active conduits of terrestrial sediment from the Rio Doce to the continental slope, as they are nearly completely filled.

RESULTS

Morphology of the Rio Doce Channel System

West tributary

The west tributary is 15 km-long as measured from a lower-order confluence upslope to the confluence analysed in this work (Fig. 3A). The west tributary shows an NNW–SSE course on the upper continental slope, shifting to NW–SE at a water depth of ~ 1100 m (Fig. 3A). There is an 80 m-high morphologic step (i.e. a sudden change in thalweg slope) approximately 500 m to the west of the studied confluence (Figs. 3B and 4). At the foot of the step in thalweg slope, a 6 m-depth scour was identified (Fig. 4B). Downstream of the step, the orientation of the tributary pathway changes from NW-SE to E-W (Fig. 3B). The tributary joins the main channel at a water depth of 1405 m (Fig. 4B), with a confluence angle of 75° (Fig. 3B).

The width of the west tributary ranges from 500 to 1800 m. The tributary height changes from 20 m to 200 m. Tributary depth ranges from 950 m to 1405 m (Fig. 4A). Its gradient decreases from 2.9° in its shallowest portion, to 0.7° downstream until the step near the confluence is reached (Fig. 4A).

Main channel (east tributary and post-confluence channel)

The main channel is 42 km-long in the interpreted seismic volume (Fig. 3A). Its orientation is NNE-SSW in its shallowest portion, and changes to NE–SW at a water depth of ~ 1300 m due to the presence of a growing salt diapir (Fig. 3A). At a water depth of 1330 m, the general orientation of the channel system changes to nearly N–S and is maintained toward the southern limit of the seismic volume (Fig. 3A). Its width changes from 200 to 1000 m, whereas its height ranges between 10 and 150 m (Qin et al., 2016). The depth of the main channel varies from 1000 to 1700 m (Fig. 4A) and the channel gradient ranges from 1.5° in its shallowest part, to 0.5° downstream (Fig. 4A).

Depositional patterns near the confluence

The depositional ratio (CSA_D/CSA_E) of the main channel (east tributary and post-confluence channel) increases by 14% downstream of the confluence and is the largest for 4 km, between 18 km and 22 km (Fig. 5A). It varies between 72% and 85%, with an average value of 78% from 18 km to 22 km (Fig. 5A). It is less than ~60% on average in the first 18 km, and approximately 50% on average between 22 km and 34 km. In addition, CSA_E and CSA_D are both larger downstream of the confluence when compared to other parts of the channel system, suggesting that the largest sediment volumes occur immediately downstream of the confluence (Fig. 5B).

Three large depositional bars are observed where the largest depositional ratios are recorded - from 18 km to 22 km along the main channel (Figure 5C). Seismic data show these deposits to be associated with lateral channel migration (Fig. 6). Channel-form erosional truncations at the base of the channel system represent the positions of previous channel banks (Fig. 6).

Lateral channel migration, demonstrated by the trajectories of shifts in bank positions (Fig. 6), resulted in large CSA_E and CSA_D values from 18 to 22 km (Fig. 5B). These large values in CSA_E and CSA_D are associated with cut-bank erosion and inner-bank deposition caused by lateral migration, respectively. We interpret that the enhanced sediment volumes in the channel system, downstream of the confluence, result from large sediment inputs from the west tributary (Fig. 5). We also interpret that flows from the east tributary contributed to deposition near the confluence, but they were not as important as the flows sourced from the west tributary. If flows from the east tributary were the main source of sediment downstream of the confluence, we would expect a reduction in channel gradient immediately downstream of the east tributary, as sediment tends to deposit in places where channel slope decreases (e.g. Friedmann et al., 2000; Mulder and Alexander, 2001; Wynn et al., 2012). Such a reduction in channel gradient, however, is not observed in association with the east tributary (Fig. 4).

The depositional ratio (CSA_D/CSA_E) decreases from 85% to 32% at a down-channel distance of 23 km (Fig. 5A), indicating that some of the sediment sourced from the west tributary was deposited directly downstream of the confluence, with only a small volume of sediment reaching the lower part of the channel system.

Temporal variations in confluence morphology

Variations in the pathway of the west tributary and the main channel

Temporal variations in channel pathways were reconstructed in Figure 7. The map of the original and present-day channels in the Rio Doce Channel System reveals significant variations in the pathway of the main channel immediately downstream of the confluence (Fig. 7A). At the confluence, a channel bend curved initially toward the west but subsequently changed its curvature to the east until the present day (Figs. 7B and 7C). In addition, sharp variations in the pathway(s) of the main channel are observed in two bends further downstream (Fig. 7). These variations increased channel sinuosity from 1.11 for the original channel pathway, to 1.72 for the present-day pathway (Figs. 7B and 7C). Seismic data show that such a significant change in channel sinuosity resulted from lateral channel migration near the confluence (Fig. 6).

The west tributary shows small changes in its pathway with time. This tributary migrated laterally for ~500 m toward the east, accompanying confluence migration (Fig. 8).

Confluence migration

In the west tributary, a step in thalweg slope and a scour are observed the west of the present-day confluence (Figs. 3B and 4B). These two features are commonly found at confluences where tributaries join the main channels (Best, 2008). Considering that the step in thalweg slope is located at the intersection of the west tributary and original pathway of the main channel (Fig. 8A), we interpret it as marking the original position of the confluence between the west and east tributaries (Fig. 8B). The different positions between the original and the present location of the confluence suggests confluence migration toward the east in the order of ~500 m.

At the original location of the confluence, the confluence bed is discordant because the west tributary is much higher than the east tributary (Fig. 8A). In contrast, the confluence bed is concordant at its present-day location, as shown by the same depth between the beds of the west and east tributaries (Fig. 4B).

Confluence bed morphology changed from discordant to concordant during confluence migration. When the west tributary started to move eastward, its bed changed from the top of the step to its foot, where its depth is similar to the bed of the east tributary. This resulted in the formation of a concordant confluence.

DISCUSSION

This work shows that the main channel bend curved toward the west at the original location of the confluence (Figs. 8 and 9). After the west tributary joined the main channel, sediment flows from the west tributary pushed the bend toward the east due to flow inertia, resulting in confluence migration and a series of morphologic and sedimentologic changes. These include changes in channel pathways, the formation of depositional bars and relative increases in sediment volume downstream of the confluence (Figs. 8 and 9).

Confluence morphology

Similarly to the confluence morphology documented in this work, Paull et al (2011) observed a step in the thalweg slope of the Soquel channel (offshore California) upstream of its confluence with the Monterey channel. A 500 m-long, smooth tributary segment was mapped between the step and the confluence, and later defined as an “embayment” at the mouth of tributary (see Fig. 8 in Paull et al., 2011). We suggest that this embayment was formed by the upstream migration of the step by means of retrogressive (headwall) erosion, contrasting with the downstream migration recorded in the study area due to the absence of features such as the original channel pathways and attached depositional bars near the confluence analyzed in the Rio Doce Channel System. An arcuate feature at the tributary mouth of the Soquel Canyon also indicates sediment failure (Paull et al., 2011). Such types of feature are not observed in the study area.

Confluence migration is also common in both meandering and braided rivers (Dixon et al., 2018). In meandering rivers of Argentina and USA, confluence migration was promoted by the migration and cut-off of tributaries, with the planform of the main channel recording minor changes (Dixon et al., 2018). In the Pliocene-Quaternary Rio Doce Channel System, confluence migration was also associated with lateral migration of the main channel, but considered to have resulted from turbidity currents flowing from the west tributary toward the east.

Generation of depositional bars

In the study area, depositional bars are identified both upstream and downstream of the confluence (Fig. 5C). Similar bars have been documented in fluvial channel confluences due to flow stagnation upstream of the confluence and flow separation downstream (Best, 1988). Flow stagnation results from mutual flow deflections away from the upstream confluence corner when flows join together (Best, 1987). Flow separation occurs when tributary flows detach from tributary banks as they enter the main channel, resulting in a zone of low velocity favouring sediment deposition (Best and Reid, 1984). Despite the different flow properties of turbidity currents (sediment gravity flows) and river currents (fluid gravity flows) (Kolla et al., 2007), flow stagnation and separation can also occur in submarine confluences and contribute to the formation of depositional bars. This is suggested by the similar locations of depositional bars in both submarine and river confluences.

Flow deflection and reflection probably occurred near the confluence in this study. A possible scenario is that the basal, denser part of turbidity currents were deflected against the inner bend of the main channel, resulting in bank erosion, whereas the upper, less dense part of the flows was reflected back to the outer bend of the main channel, leading to bank deposition and the formation of depositional bars (Fig. 9). After these bars were formed, subsequent tributary flows were deflected to promote bank erosion and deposition, leading to further growth of the bars. Finally, channel gradient decreased as the channel became longer and more sinuous, leading to enhanced deposition near the confluence.

Flows within the channel system

The lack of core data and age constraints make it difficult to evaluate flow dynamics within the Rio Doce Channel System. Nevertheless, variations in the continuity and amplitude of seismic reflections in submarine channels have been widely used to assess flow dynamics in a qualitative way. For example, active channels are characterised by high-amplitude near-seafloor strata, whereas inactive channels are commonly of relative low amplitude (Pirmez et al., 2000; Gamboa et al., 2012; Jobe et al., 2015; Hansen et al., 2017). In the study area, the west tributary and main channel are likely active at present based on the presence of high-amplitude strata inside them (Gamboa et al., 2012). Therefore, flows downstream of the confluence could be either sourced from the west tributary or the east tributary, or from both at the same time.

We interpret that the west tributary contributed with larger volumes of sediment to the post-confluence channel than the east tributary due to the presence of large depositional bars downstream of the confluence. In addition, there are abrupt decreases in channel width and height (Qin et al., 2016) and a temporal change in the channel pathway immediately downstream of the confluence (Fig. 7A). All these changes suggest a marked effect of the west tributary on post-confluence channel morphology during the main stages of confluence migration (Fig. 9). However, based on the smooth transition at the confluence between the east tributary and the post-confluence channel, the east tributary is currently active (Fig. 4B).

The west tributary contributed more sediments than the east tributary to the confluence region, suggesting an eastern ward shift in major sediment sources on the continental shelf (Figs. 9A and B). Such a shift is interpreted to be a result of variations in sedimentary processes on the continental shelf. Similar variations in tributary activities have also been documented offshore Niger delta (Jobe et al., 2015; Hansen et al., 2017). These variations have been linked to river avulsions on the Niger delta (Jobe et al., 2015) and the capture of sediment supply by different canyons along the Niger shelf edge (Hansen et al., 2017). In this work, both of scenarios mentioned above could have occurred as the sediment delivery processes from the Rio Doce delta to the submarine channels is still unclear.

Lateral migration as a response to turbidity currents from the west tributary

We suggest that the west tributary provided significant volumes of sediment into the post-confluence channel, as indicated by large depositional bars immediately downstream of the confluence. Lateral channel migration was a major response to greater sediment discharge and resulted in confluence migration, as shown by: a) the multiple channel forms in depositional bars downstream of the confluence, and b) the higher magnitude of lateral migration at the three meander bends downstream of the confluence (Fig. 6).

In a channel system offshore Nigeria, Jobe et al., (2015) found a transition from large-scale lateral migration at the early incision stage, to aggradation soon after, and attributed this transition to a decrease in sediment discharge. Unfortunately, it is difficult of evaluate the role of extrinsic controls (e.g. climate change, tectonic activity, and the proximity of a shelf-edge delta) in sediment delivery to the channel system due to the lack of chronostratigraphic constraints (Jobe et al., 2015). In subaerial settings, close relationships between sediment supply and lateral channel migration have also been documented. For example, downstream of tributaries a relative increase in channel migration rate is observed in rivers such as the Amazon (e.g. at the confluence between the Rio Mamoré and Rio Grande) due to high sediment load from tributaries and associated point-bar growth (Constantine et al., 2014).

Other flow properties such as flow velocity could have also contributed to lateral channel migration in the study area. Numerical models by Das et al. (2004) show that lateral migration is more likely to be driven by erosional currents with a relatively high current velocity and a steep channel bed slope. Ismail (2017) further found that higher junction angles result in higher peak front velocity in channel flows. In this work, the junction angle is 75°, which is a higher angle than that reported by Ismail (2017). Therefore, a relatively high flow velocity likely promoted out-bank erosion during lateral channel migration.

Hubbard et al. (2009) suggest a link between the grain size of turbidity currents and the magnitude of lateral channel migration in the Molasse foreland basin of Austria. They considered relative pauses in channel sedimentation (Puchkirchen Formation, represented by 1–20 m thick shale beds), and associated slow channel migration rates, as reflecting the cessation of coarse-grained sediment supply. Similarly, Nelson and Dubé (2016) found a close relationship between river bed sediment flux and lateral channel mobility in the Chehalis River in Washington State, Northeast USA. The influx of coarse-grained sand may have also contributed to lateral migration in the Rio Doce Channel System, but it is hard to confirm such an assumption without sediment cores and in-situ current monitoring equipment.

CONCLUSIONS

This work documents a series of morphologic and sedimentologic features downstream of a confluence of a Pliocene-Quaternary submarine channel system, SE Brazil. Such variations are interpreted as resulting from the effect of turbidity currents sourced from tributaries, which have impacted on the hydrodynamic processes sculpting a submarine confluence. The results of this work can be summarized as follows:

(1) High-quality 3D seismic data reveal confluence migration approaching 500 m during the development of the Pliocene-Quaternary Rio Doce Channel System. The original location of the confluence is discordant, and marked by an 80 m-high morphologic step. At present, the confluence is concordant, i.e., characterized by a similar bed depth between the tributary and the main submarine channel.

(2) Significant temporal changes are recorded in the pathway of the main channel and associated sinuosity values. At the confluence, a channel bend in the main channel curved toward the west

when the bend was formed in the Pliocene. However, this same channel bend curves toward the east at present. We interpret the changes in the geometry of this bend as resulting from the effect of turbidity currents sourced from the west tributary. Turbidity currents deviated the channel bend and curved it toward the east. Two other bends downstream of the confluence also show significant variations in channel pathway, increasing the sinuosity of the main channel from 1.11 to 1.72.

(3) Lateral channel migration is therefore proposed as an important process responding to sediment supply from channel tributaries. Lateral channel migration led, in the study area, to the accumulation of large depositional bars fed by sediment discharged from tributaries.

(4) Confluence evolution in this study reflects an eastward shift in sediment sources at the continental shelf. The cause of such a shift is interpreted as reflecting variations in sedimentary processes on the continental shelf. Further numerical and physical models addressing the hydrodynamic processes at submarine confluences are needed to further understand how these latter evolve. Both numerical and physical models are important to understand flow properties (e.g. sediment discharge, grain size, flow velocity) and associated variations in morphology and architecture (e.g. depositional bars formed during lateral channel migration) of submarine channel systems.

ACKNOWLEDGEMENTS

The authors thank CGG for the permission to use the 3D seismic data in this article. Luke Pettinga, an anonymous reviewer and associated editor Ganqing Jiang are acknowledged for their constructive comments. Yongpeng Qin thanks the financial support from 'The National Major Science and Technology Program (2017ZX05026006)' and NSFC-Guangdong Joint Foundation (U1701245). Davide Gamboa thanks the Sêr Cymru National

Research Network for Low Carbon Energy and the Environment and publishes with the permission of the Executive Director, British Geological Survey.

REFERENCES CITED

Alves, T.M., Cartwright, J., and Davies, R.J., 2009, Faulting of salt-withdrawal basins during early halokinesis: Effects on the Paleogene Rio Doce Canyon system (Espirito Stanto Basin, Brazil): American Association of Petroleum Geology Bulletin, v. 93, p. 617-652, doi:10.1306/02030908105

Amante, C., and Eakins, B.W., 2009. ETOPO1 1 Arc-Minute Global Relief Model: Procedures, Data Sources and Analysis. NOAA Technical Memorandum NESDIS NGDC-24. National Geophysical Data Center, NOAA. doi:10.7289/V5C8276M.

Atwater B.F. Carson B. Griggs G.B. Johnson H.P. and Salmi M.S., 2014, Rethinking turbidite paleoseismology along the Cascadia subduction zone: Geology, v. 42, p. 827–830, doi:10.1130/G35902.1.

Best JL., 1987, Flow dynamics at river channel confluences: Implications for sediment transport and bed morphology, *in* Etheridge, F.G., Flores, R.M., Harve, M.D., eds., Recent Developments in Fluvial Sedimentology: Society of Economic Paleontologists and Mineralogists, Special Publication v. 39, p. 27–35, doi:10.2110/pec.87.39.0027.

Best, J., L., and Reid, I., 1984, Separation Zone at Open - Channel Junctions: Journal of Hydraulic Engineering, v. 10, p. 1588-1594, doi:10.1061/(ASCE)0733-9429(1984)110:11(1588).

Best, J.L., 1988, Sediment transport and bed morphology at river channel confluences: Sedimentology, v. 35, p. 481-498, doi: 10.1111/j.1365-3091.1988.tb00999.x.

Bischoff, A., and Lipsky, M., 2008. Estilos arquiteturais de turbiditos na Bacia do Espírito Santo. III Simpósio Brasileiro da SBGf, Belém, Brazil.

Constantine, J., A., Dunne, T., Ahmed, J., Legleiter, C., and Lazarus, E.D., 2014, Sediment supply as a driver of river meandering and floodplain evolution in the Amazon Basin: Nature Geoscience, v. 7, p. 899–903, doi:10.1038/ngeo2282.

Das, H.S., Imran, J., Pirmez, C., and Mohrig, D., 2004, Numerical modeling of flow and bed evolution in meandering submarine channels: Journal of Geophysical Research, v. 119, C10009, doi:10.1029/2002JC001518

Dixon, S.J., Sambrook, S.G., Best, J.L., Nicholas, A.P., Bull, J.M., Vardy, M.E., Sarker, M.H., and Goodbred, S., 2018, The planform mobility of river channel confluences: Insights from analysis of remotely sensed imagery: Earth Science Review, v. 176, p. 1–18, doi:10.1016/j.earscirev.2017.09.009.

Ferguson, R., and Hoey, T., 2008, Effects of tributaries on main-channel geomorphology, *in* Rice, S.P., Roy, A.G., Rhoads, B.L., eds., River Confluences, Tributaries and the Fluvial Network: Wiley, London, p. 183-208.

Fiduk, J.C., Brush, E.R., Anderson, L.E., Gibbs, P.B., and Rowan, M.G., 2004, Salt deformation, magmatism, and hydrocarbon prospectivity in the Espirito Santo Basin, offshore Brazil, *in* Post, P.J., et al. eds., Salt-sediment Interactions and Hydrocarbon Prospectivity: Concepts, Applications, and Case Studies for the 21st Century: GCSSEPM 24th Annual Research Conference, p. 370-392.

França, R.L., Del Rey, A.C., Tagliari, C.V., Brandão, J.R., and De Rossi Fontanelli, P., 2007, Bacia do Espírito Santo. Boletim de Geociencias da Petrobras, v. 15, p. 501-509.

Friedmann, S.J., Beaubouef, R.T., Pirmez, C., and Jennette, D.C., 2000, The effects of gradient changes on deep-water depositional systems: an integrated approach: American Association of Petroleum Geologists Annual Meeting, New Orleans, U.S, p. 51.

Gamboa, D., and Alves, T.M., 2015, Spatial and dimensional relationships of submarine slope architectural elements: A seismic-scale analysis from the Espírito Santo Basin (SE Brazil): Marine and Petroleum Geology, v. 64, p. 43-57, doi:10.1016/j.marpetgeo.2015.02.035.

Gamboa, D., Alves, T.M., and Cartwright, J., 2012, A submarine channel confluence classification for topographically confined slopes: Marine and Petroleum Geology, v. 35, p. 176-189, doi:10.1016/j.marpetgeo.2012.02.011.

Goldfinger, C., 2011, Submarine paleoseismology based on turbidite records: Annual Review of Marine Science, v. 3, p. 35–66, doi:10.1146 /annurev-marine-120709-142852.

Greene, H. G., Maher, N.M., and Paull, C.K., 2002, Physiography of the Monterey Bay National Marine Sanctuary and implications about continental margin development: Marine Geology, v. 181, p. 55-82, doi:10.1016/S0025-3227(01)00261-4.

Hansen, L., Janocko, M., Kane, I., and Kneller, B., 2017, Submarine channel evolution, terrace development, and preservation of intra-channel thin-bedded turbidites: Mahin and Avon channels, offshore Nigeria: Marine Geology, v. 383, p. 146-167, doi:10.1016/j.margeo.2016.11.011.

Hubbard, S.M., De Ruig, M.J., and Graham, S.A., 2009, Confined channel-levee complex development in an elongate depocenter: deep-water Tertiary strata of the Austrian Molasse Basin: Marine and Petroleum Geology, v. 26, p. 85-112, doi: 10.1016/j.marpetgeo.2007.11.006.

Ismail, H., 2017, Confluence of density currents produced by lock-exchange. PhD thesis, University of South Carolina. 1-92.

Jobe, Z.R., Sylvester, Z., Parker, A.O., Howes, N., Slowey, N., and Pirmez, C., 2015, Rapid adjustment of submarine channel architecture to changes in sediment supply: Journal of Sedimentary Research, v. 85, p. 729–753, doi:10.2110/jsr.2015.30.

Jonell, T.N., Carter, A., Böning, P., Pahnke, K., and Clift, P.D., 2017. Climatic and glacial impact on erosion patterns and sediment provenance in the Himalayan rain shadow, Zanskar River, NW India. Geological Society of America Bulletin, v. 129, p. 820–836, doi:10.1130/B31573.1.

Kolla, V., Posamentier, H.W., and Wood, L.J., 2007. Deep-water and fluvial sinuous channels: characteristics, similarities and dissimilarities, and modes of formation. Marine and Petroleum Geology, 24, 388-405, doi: 10.1016/j.marpetgeo.2007.01.007

Lima, J.E.F.W., Lopes, W.T.A., De Carvalho, N.O., Vieira, M.R., and Da Silva, E.M., 2005, Suspended sediment fluxes in the large river basins of Brazil, in: Walling, D.E., Horowitz, A.J., eds., Sediment Budgets 1, Proceedings of the Foz do Iguacu Symposium, April 2005, IAHS Publication, vol. 291, IAHS Press, Wallingford, UK (2005), p. 355–363

Micallef, A., Mountjoy, J.J., Barnes, P.M., Canals, M., and Lastras, G., 2014, Geomorphic response of submarine canyons to tectonic activity: insights from the Cook Strait canyon system, New Zealand: Geosphere, v. 10, p. 905-929, doi:10.1130/GES01040.1

Mitchell, N.C., 2004, Form of submarine erosion from confluences in Atlantic USA continental slope Canyons: American Journal of Science, v. 304, p. 590-611, doi:10.2475/ajs.304.7.590.

Mohriak, W.U., Nemcok, M., and Enciso, G., 2008, South Atlantic divergent margin evolution: riftborder uplift and salt tectonics in the basins of Southeastern Brazil, in Pankhurst, R.J., Trouw, R.A.J., Brito Neves, B.B., De Wit, M.J., eds., West Gondwana Pre-Cenozoic Correlations across the South Atlantic Region: Geological Society of London, Special Publication, 294, p, 365-398, doi:10.1144/SP294.19.

Mulder, T., and Alexander, J., 2001, Abrupt change in slope causes variation in the deposit thickness of concentrated particle-driven density currents: Marine Geology, v. 175, p. 221–235, doi:10.1016/S0025-3227(01)00114-1.

Munack, H., Korup, O., Resentini, A., Limonta, M., Garzanti, E., Blöthe, J.H., Scherler, D., Wittmann, H., and Kubik, P.W., 2014, Postglacial denudation of western Tibetan Plateau margin outpaced by long-term exhumation: Geological Society of America Bulletin, v. 126, p. 1580–1594, doi:10.1130/B30979.1

Munoz, S.E., Giosan, L., Blusztajn, J., Rankin, C., and Stinchcomb, G.E., 2019, Radiogenic fingerprinting reveals anthropogenic and buffering controls on sediment dynamics of the Mississippi River system; Geology, doi: https://doi.org/10.1130/G45194.1.

Nelson, A., and Dubé, K., 2016, Channel response to an extreme flood and sediment pulse in a mixed bedrock and gravel-bed river: Earth Surface Processes and Landforms, v. 41, p, 178-195, doi:10.1002/esp.3843.

Noda, A., TuZino, T., Furukawa, R., Joshima, M., and Uchida, J.I., 2008, Physiographical and sedimentological characteristics of submarine canyons developed upon an active forearc slope: The Kushiro Submarine Canyon, northern Japan: Geological Society of America Bulletin, v. 120, p. 750–767, doi:10.1130/B26155.1.

Ojeda, H.A.O., 1982, Structural framework, stratigraphy, and evolution of Brazilian marginal basins: American Association of Petroleum Geology Bulletin, v. 66, p. 732-749.

Oliveira, E.N.D., Knoppers, B.A., Lorenzzetti, J.A., Medeiros, P.R.P., Carneiro, M.E., and Souza, W.F.L.D., 2012, A satellite view of riverine turbidity plumes on the NE–E Brazilian coastal zone. Brazilian Journal of Oceanography, v. 60, p. 283–298, doi:10.1590/S1679-87592012000300002.

Paull, C.K., Caress, D.W., Ussler, W., Lundsten, E., and Meiner-Johnson, M., 2011, High-resolution bathymetry of the axial channels within Monterey and Soquel submarine canyons, offshore central California: Geosphere, v, 7, p, 1077–1101, doi:10.1130/GES00636.1.

Pirmez, C., Beaubouef, R.T., Friedmann, S.J. and Mohrig, D.C., 2000, Equilibrium profile and baselevel in submarine channels: examples from Late Pleistocene systems and implications for the architecture of deepwater reservoirs: Deepwater Reservoirs of the World, GCSSEPM Foundation 20th Annual Research Conference, p, 782–805.

Qin, Y., Alves, T.M., Constantine, J., and Gamboa, D., 2016, Quantitative seismic geomorphology of a submarine channel system in SE Brazil (Espírito Santo Basin): Scale comparison with other submarine channel systems: Marine and Petroleum Geology, v. 78, p. 455-473, doi:10.1016/j.marpetgeo.2016.09.024.

Summerhayes, C.P., De Melo, U., and Barretto, H.T., 1976, The influence of upwelling on suspended matter and shelf sediments off southeastern Brazil: Journal of Sedimentary Research, v. 46, p. 819-828, doi:10.1306/212F7068-2B24-11D7-8648000102C1865D.

Wynn, R.B., Talling, P.J., Masson, D.G., Le Bas, T.P., Cronin, B.T., and Stevenson, C.J., 2012, The Influence of Subtle Gradient Changes on Deep-water Gravity Flows: A Case Study from the Moroccan Turbidite System, SEPM Spec. Publ. 99, p. 371-383, doi:10.2110/pec.12.99.0371.

FIGURE CAPTIONS

Fig. 1. (A) Bathymetric and topographic map of the SE Brazilian margin showing the location of the study area in the Espírito Santo Basin. (B) Contoured seafloor map of the study area generated from the interpreted seismic volume. Bathymetric data in (A) was taken from GeoMapApp (http://www.geomapapp.org; Amante and Eakins, 2009).

Fig. 2. Uninterpreted and interpreted seismic profiles highlighting the areas of the Pliocene-Quaternary Rio Doce Channel System used to calculate CSA_E (cross-sectional area of the channel system formed by erosional processes) and CSA_D (cross-sectional area of the deposits within the channel system). (modified from Qin et al., 2016). Overbank deposits were not considered in the calculation because they may have similar seismic facies to deposits unrelated to the channel system, causing errors in calculations. The location of the seismic profile is shown in Fig. 1B. The polarity of data is SEG normal i.e., positive amplitude reflections (red) on the seismic profiles represent an increase in acoustic impedance in seismic sections.

Fig. 3. (A) Dip map of the seafloor showing that the modern Rio Doce Canyon System is composed of west and east tributaries upslope of a confluence and a post-confluence channel downslope. The east tributary and the post-confluence channel comprise the main channel. (B) Dip map showing the seafloor morphology near the confluence. In the west tributary a step in thalweg slope, with a height of 80 m, is located ~500 m to the west of the confluence, as shown in dark color.

Fig. 4. (A) Depth profiles of the west tributary and main channel. Values next to the profiles show the average channel gradient of a specific channel segment. (B) Enlarged view of depth profiles near the confluence. This graph shows a morphologic step in thalweg slope and a scour in the west tributary, near the confluence.

Fig. 5. (A) Depositional ratio (CSA_D/CSA_E) along the channel system, which comprises the east tributary and the post-confluence channel. The depositional ratio was not calculated at the confluence because here CSA_D and CSA_E are also affected by the west tributary, instead of the east tributary and main channel alone. (B) Variations of cross-sectional area of the channel system (CSA_E) and cross-sectional area of deposits within the channel system (CSA_D). These two parameters were not calculated at the confluence because they are also affected by the west tributary. (C) Thickness map of deposits within the channel system. The upper and lower surfaces used in the calculation of thickness are the sea floor and the base of the channel system, respectively.

Fig. 6. Seismic profiles across three depositional bars near the confluence. The profiles reveal lateral channel migration and suggest that depositional bars were formed by this same process. The shift in bank positions show the trajectories of lateral channel migration.

Fig. 7. (A) Schematic diagram showing significant variations in the pathway of the channel immediately downstream of the confluence. Small variations in the pathway of other parts of the main channel are also observed. (B) and (C) show that channel sinuosity increases from 1.11 to 1.17 due to pathway changes in the post-confluence channel.

Fig. 8. Schematic diagram highlighting the observed variations in the geometry of channel pathways and confluence, overlain on a seafloor dip map. (A) The step in thalweg slope at the west tributary is shown by a high dip value and dark color. The foot of the step marks the original position of the confluence. (B) Original position of the confluence at the intersection between the west tributary and the post-confluence channel. (C) Present-day position of the confluence at the intersection between the east tributary and post-confluence channel. (D) The confluence migrated

~500 m toward the east until it reached its present location.

Fig. 9. Schematic diagram summarizing the influence of the west tributary on the evolution of the Pliocene-Quaternary Rio Doce Channel System. Turbidity currents from the west tributary promoted a series of morphologic and architectural variations via lateral channel migration. These included confluence migration, the formation of three large depositional bars downstream of the confluence, changes in channel pathway, and variations in channel sinuosity. T2 and T4 correspond to Figs. 8B and 8C, respectively.

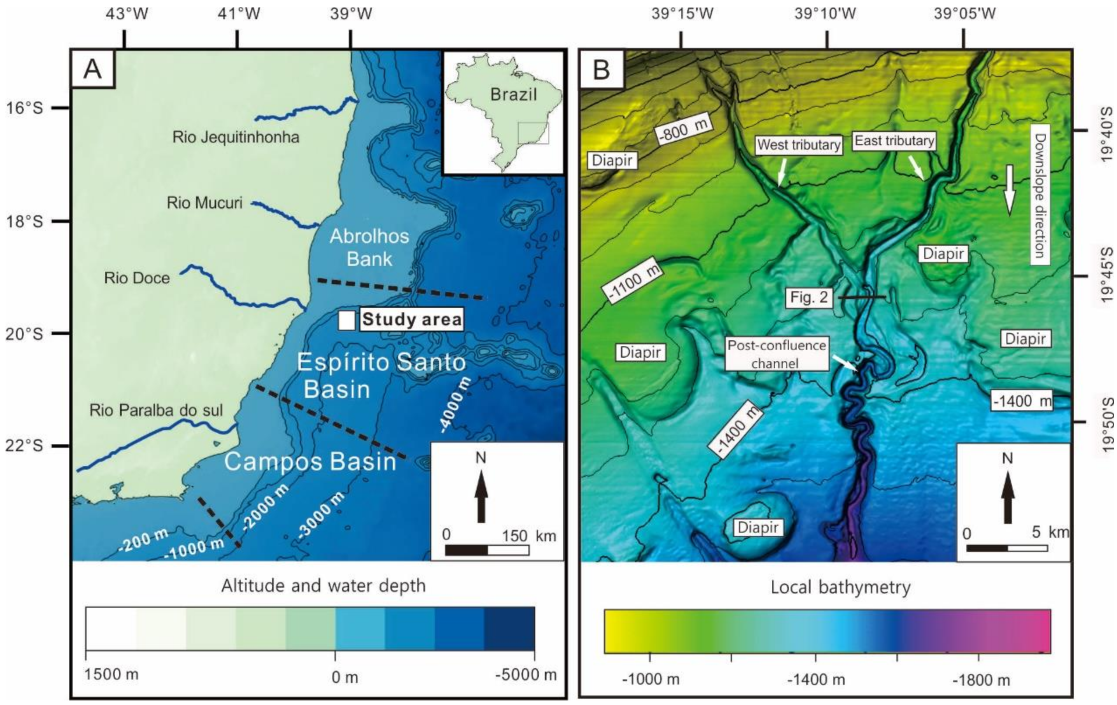
A
43°W
41°W
39°W
16°S
18°S
20°S
22°S
Brazil
Rio Jequitinhonha
Rio Mucuri
Rio Doce
Rio Paralba do sul
Abrolhos Bank
Study area
Espírito Santo Basin
Campos Basin
-200 m
-1000 m
-2000 m
-3000 m
-4000 m
N
0
150 km
Altitude and water depth
1500 m
0 m
-5000 m
B
39°15'W
39°10'W
39°05'W
19°40'S
19°45'S
19°50'S
-800 m
Diapir
West tributary
East tributary
Downslope direction
-1100 m
Fig. 2
Post-confluence channel
-1400 m
N
0
5 km
Local bathymetry
-1000 m
-1400 m
-1800 m

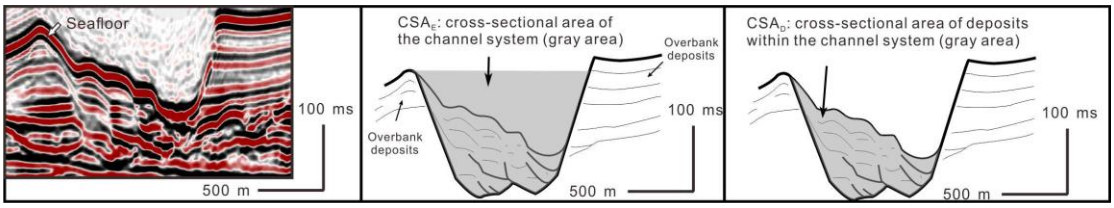

Seafloor
100 ms
500 m
CSA_E: cross-sectional area of the channel system (gray area)
Overbank deposits
Overbank deposits
100 ms
500 m
CSA_D: cross-sectional area of deposits within the channel system (gray area)
100 ms
500 m

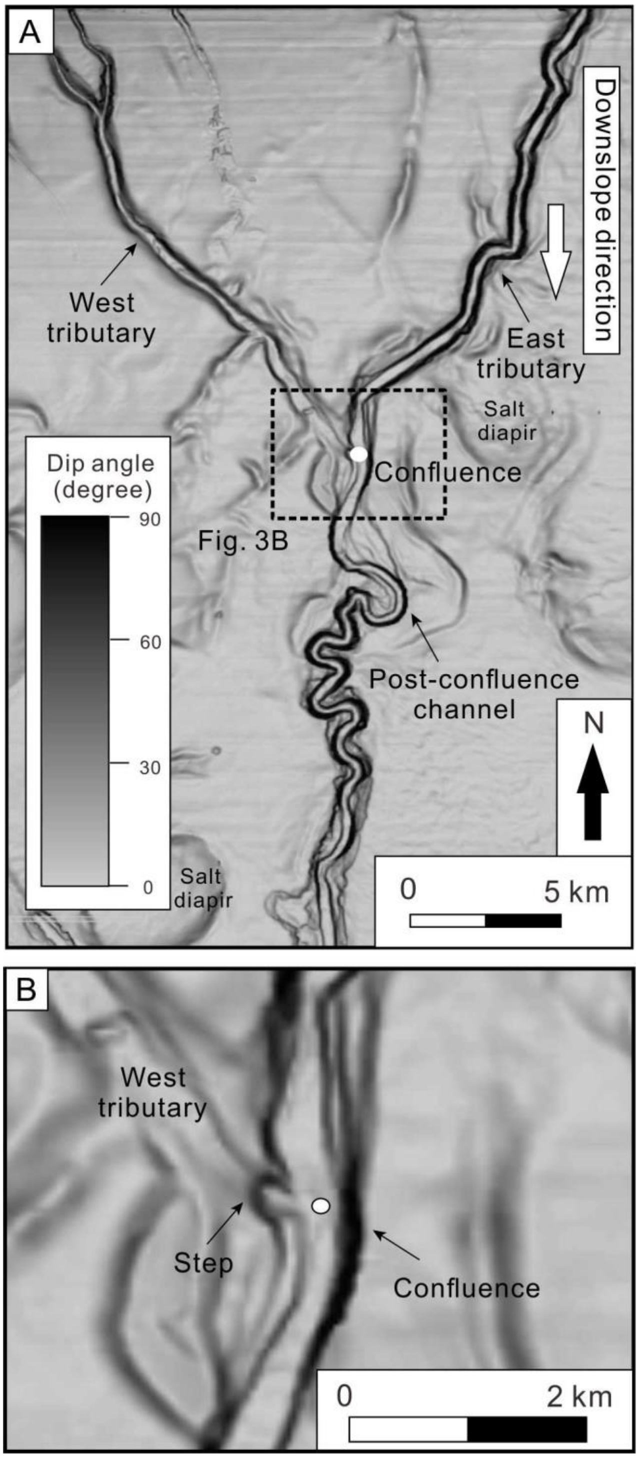
A
Downslope direction
West tributary
East tributary
Salt diapir
Confluence
Dip angle (degree)
90
60
30
0
Fig. 3B
Post-confluence channel
N
Salt diapir
0
5 km
B
West tributary
Step
Confluence
0
2 km

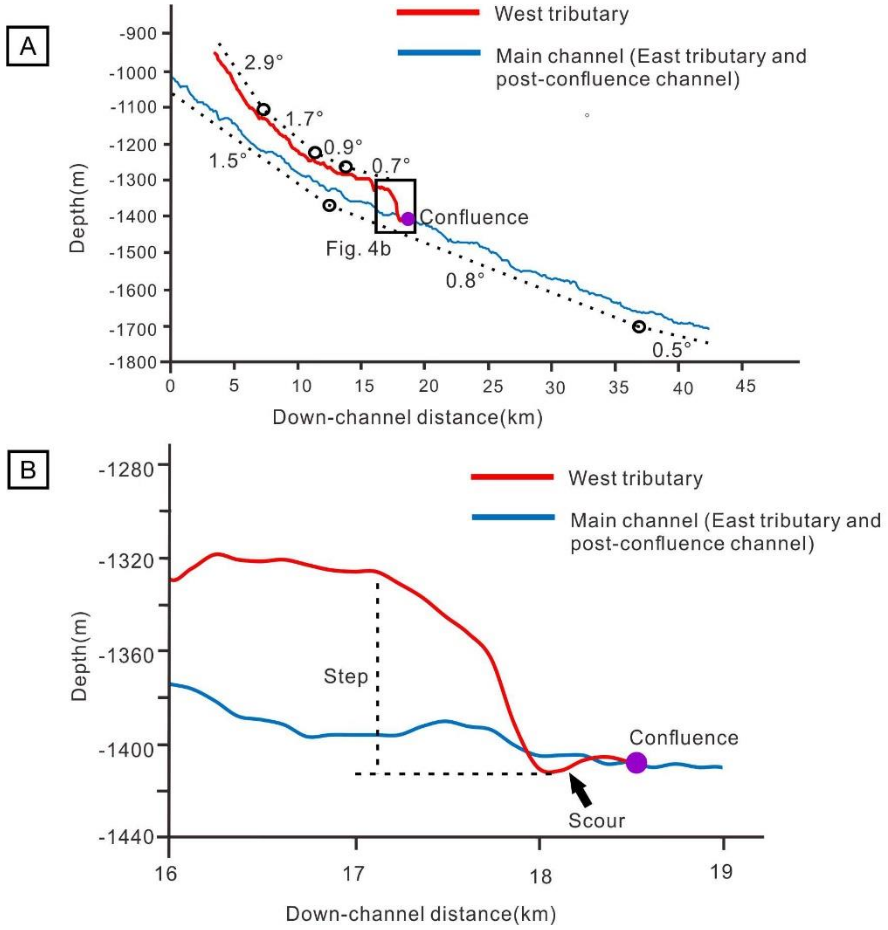
A
West tributary
Main channel (East tributary and post-confluence channel)
Depth(m)
2.9°
1.7°
0.9°
0.7°
1.5°
Confluence
Fig. 4b
0.8°
0.5°
Down-channel distance(km)
B
West tributary
Main channel (East tributary and post-confluence channel)
Depth(m)
Step
Confluence
Scour
Down-channel distance(km)

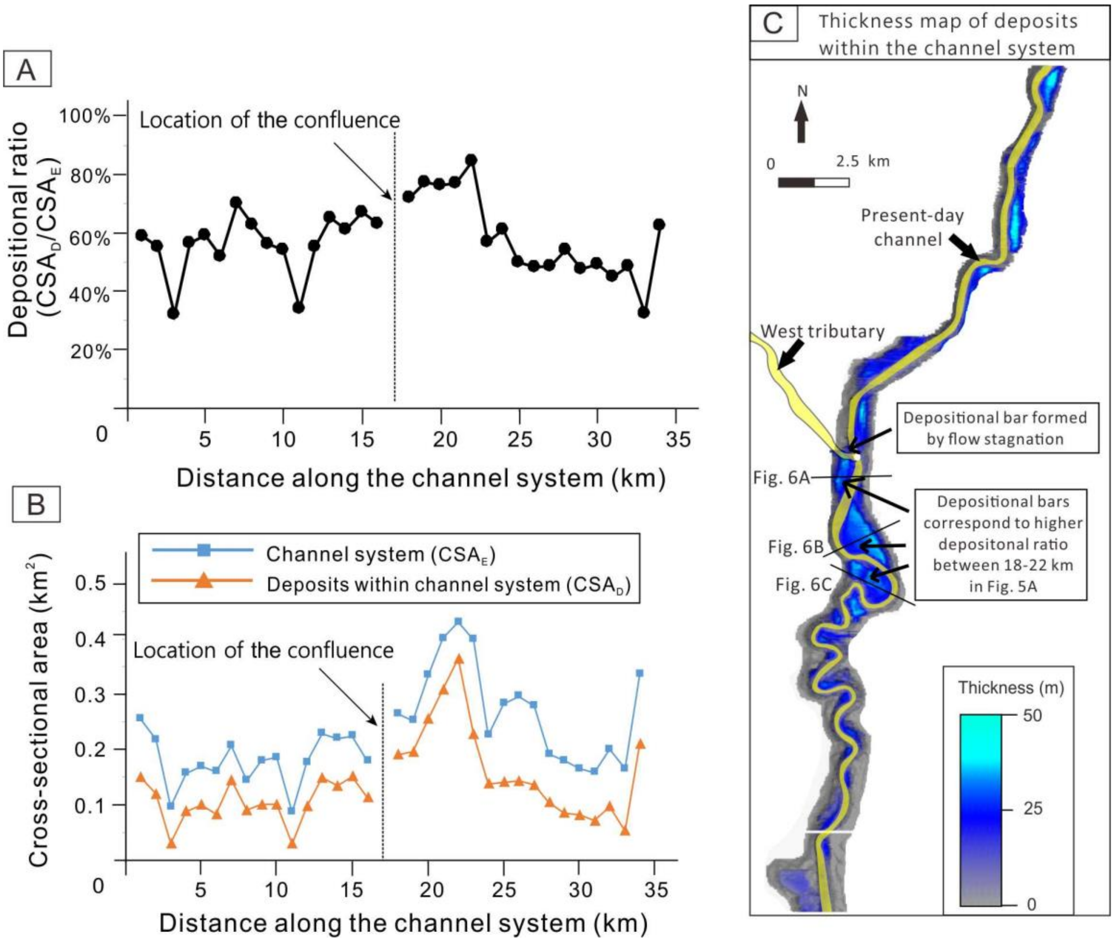
A
Location of the confluence
Depositional ratio (CSA_D/CSA_E)
Distance along the channel system (km)
B
Channel system (CSA_E)
Deposits within channel system (CSA_D)
Location of the confluence
Cross-sectional area (km^2)
Distance along the channel system (km)
C
Thickness map of deposits within the channel system
N
0
2.5 km
Present-day channel
West tributary
Depositional bar formed by flow stagnation
Fig. 6A
Fig. 6B
Fig. 6C
Depositional bars correspond to higher depositonal ratio between 18-22 km in Fig. 5A
Thickness (m)
50
25
0

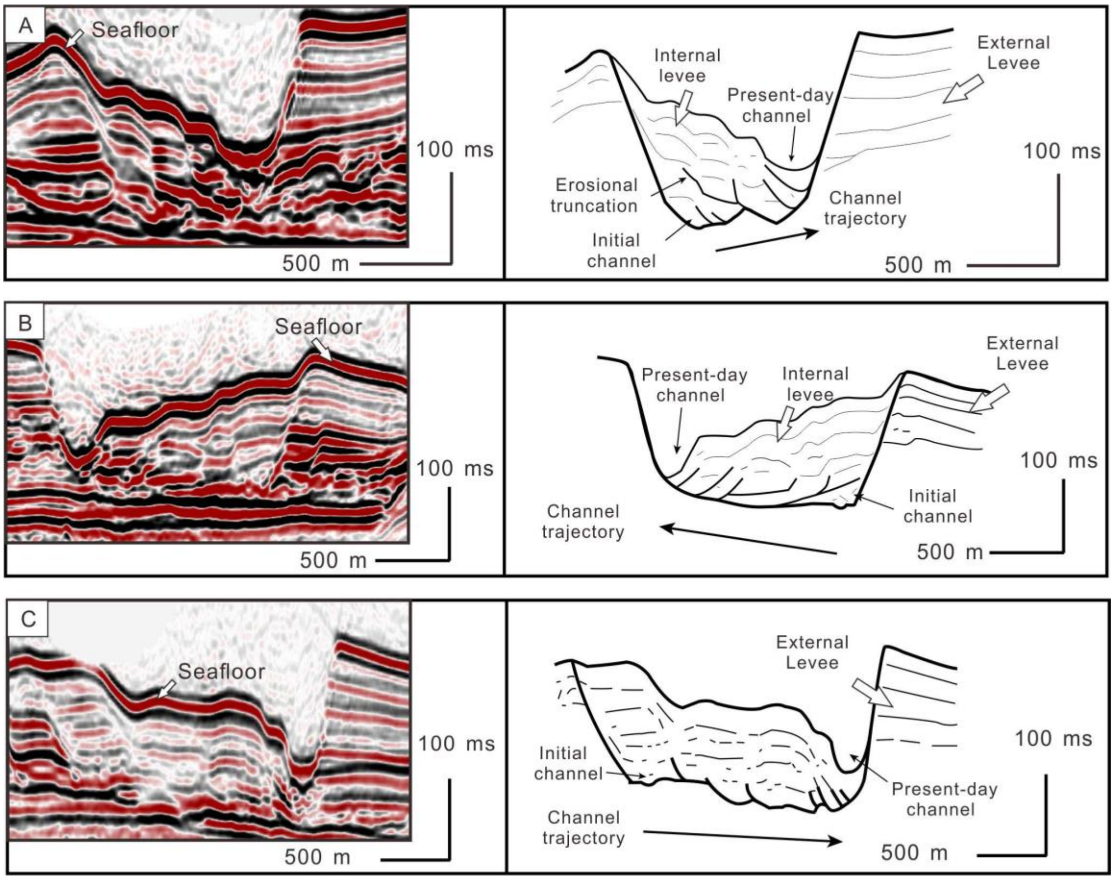
A
Seafloor
100 ms
500 m
Internal levee
Present-day channel
External Levee
Erosional truncation
Initial channel
Channel trajectory
100 ms
500 m
B
Seafloor
100 ms
500 m
Present-day channel
Internal levee
External Levee
Initial channel
Channel trajectory
100 ms
500 m
C
Seafloor
100 ms
500 m
External Levee
Initial channel
Present-day channel
Channel trajectory
100 ms
500 m

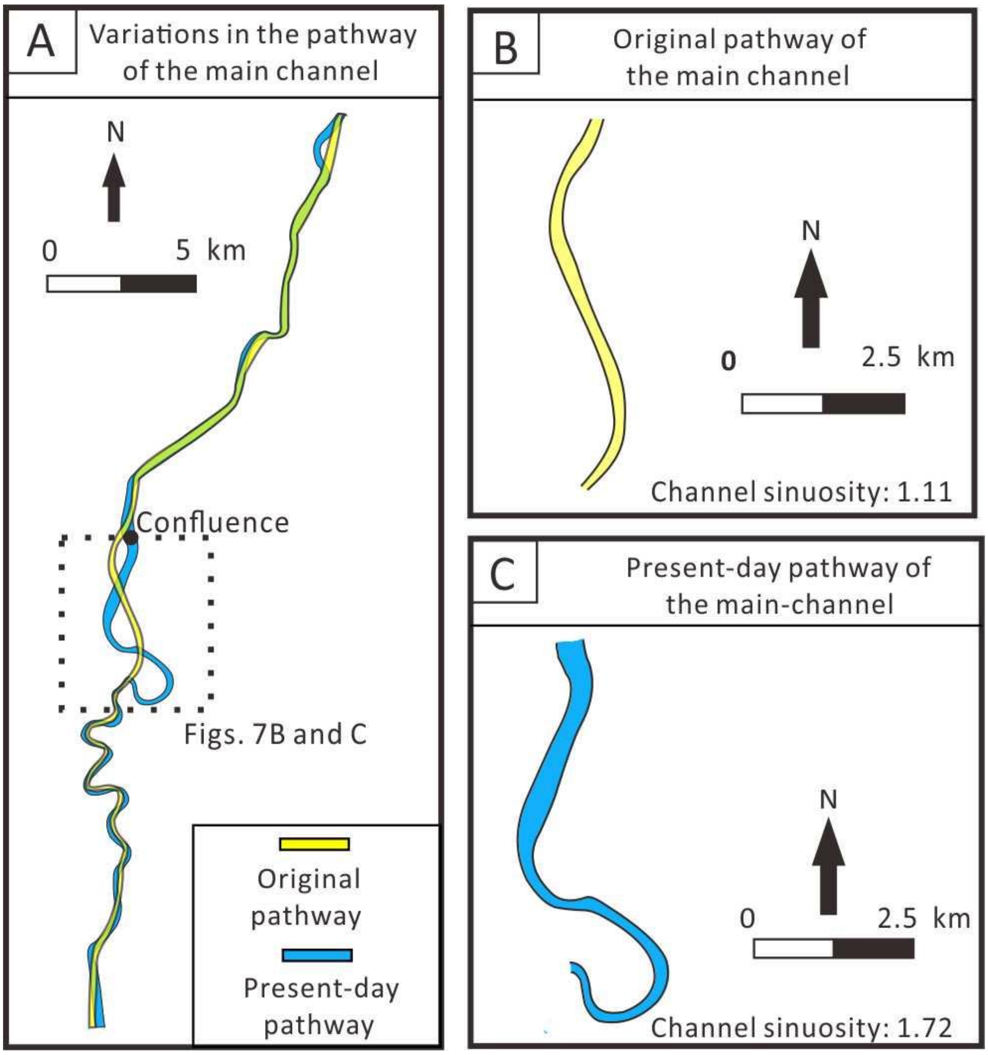
A
Variations in the pathway of the main channel
N
0
5 km
Confluence
Figs. 7B and C
Original pathway
Present-day pathway
B
Original pathway of the main channel
N
0
2.5 km
Channel sinuosity: 1.11
C
Present-day pathway of the main-channel
N
0
2.5 km
Channel sinuosity: 1.72

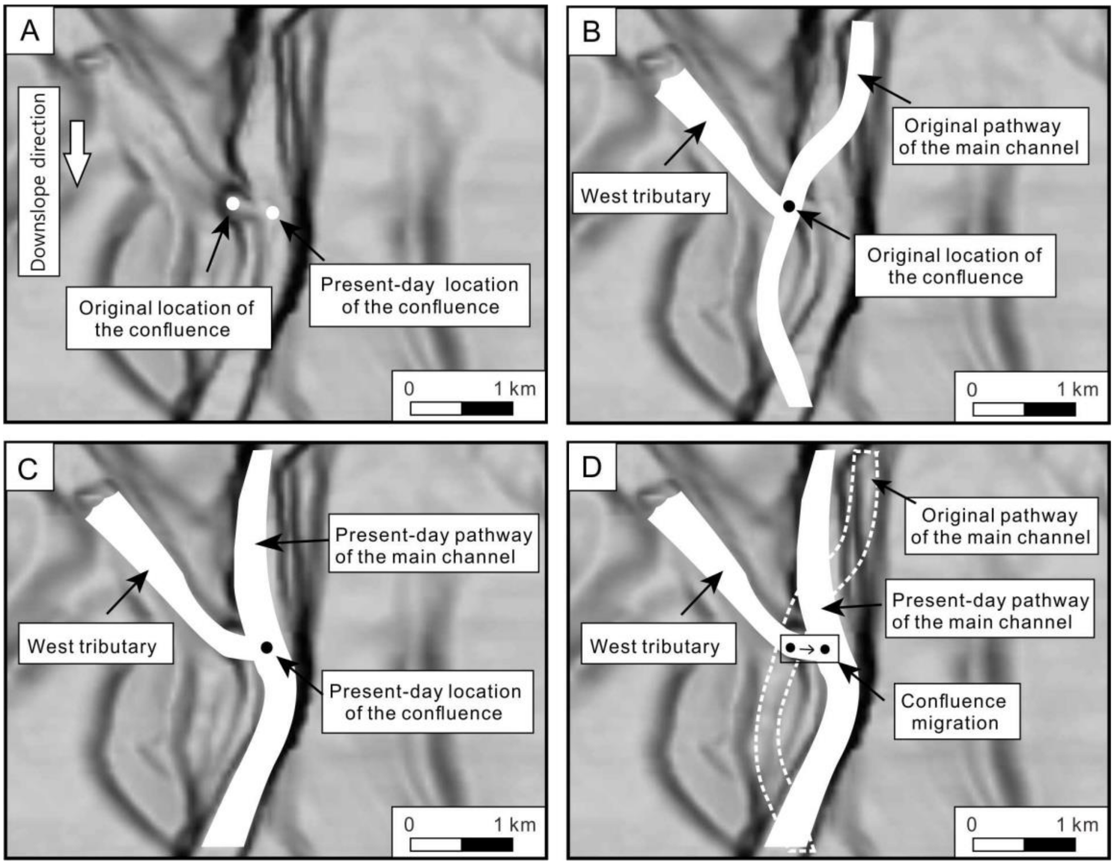
A
Downslope direction
Original location of the confluence
Present-day location of the confluence
0
1 km
B
Original pathway of the main channel
West tributary
Original location of the confluence
0
1 km
C
Present-day pathway of the main channel
West tributary
Present-day location of the confluence
0
1 km
D
Original pathway of the main channel
Present-day pathway of the main channel
West tributary
Confluence migration
0
1 km

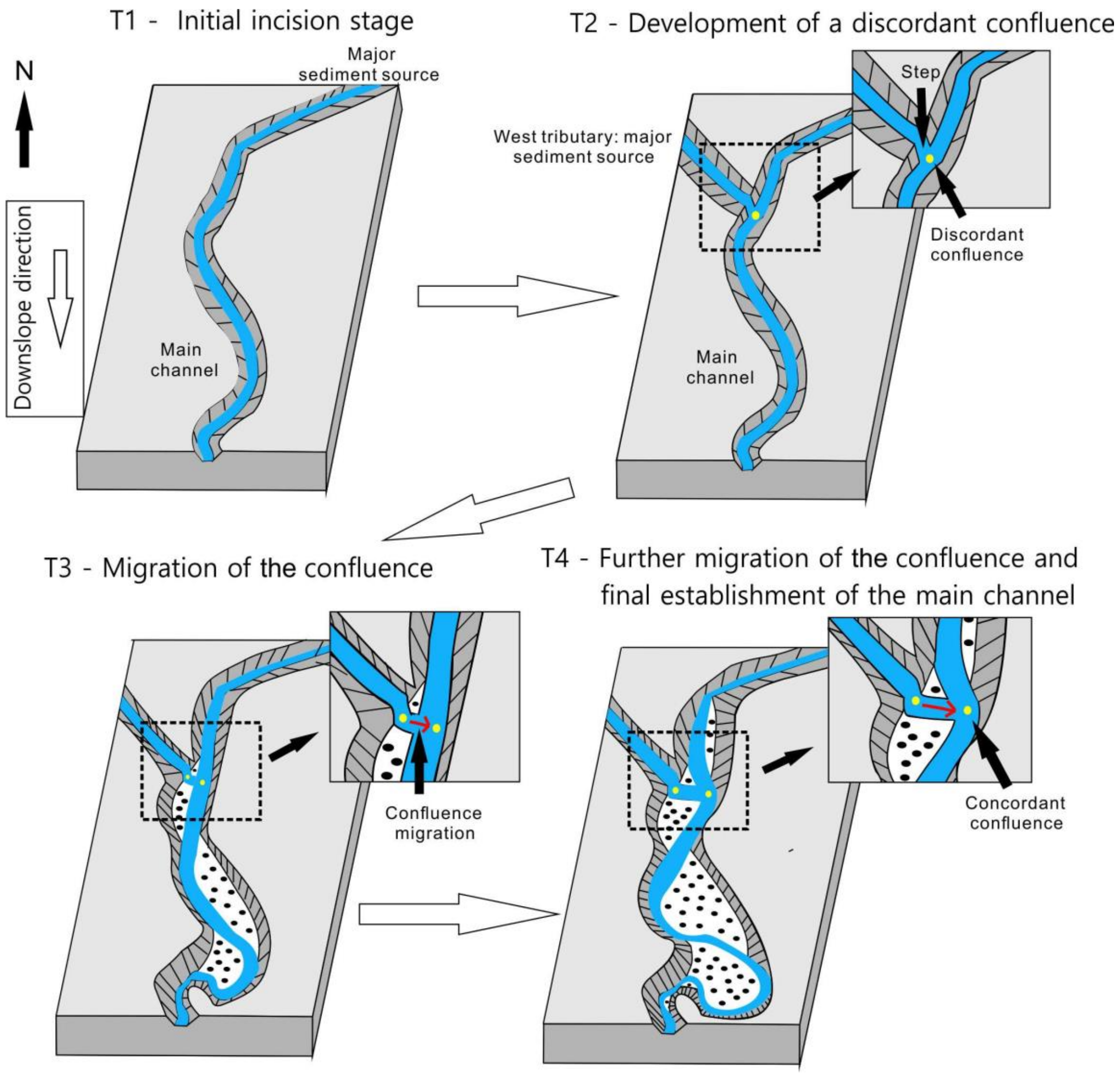
T1 - Initial incision stage
Major sediment source
N
Downslope direction
Main channel
T2 - Development of a discordant confluence
West tributary: major sediment source
Step
Discordant confluence
Main channel
T3 - Migration of the confluence
Confluence migration
T4 - Further migration of the confluence and final establishment of the main channel
Concordant confluence